



UNIVERSITY OF LEEDS

This is a repository copy of *Performance Measurements of the SAFIR Prototype Detector With the STiC ASIC Readout*.

White Rose Research Online URL for this paper:
<http://eprints.whiterose.ac.uk/143328/>

Version: Accepted Version

Article:

Ahnen, M, Becker, R, Buck, A et al. (20 more authors) (2018) Performance Measurements of the SAFIR Prototype Detector With the STiC ASIC Readout. *IEEE Transactions on Radiation and Plasma Medical Sciences*, 2 (3). pp. 250-258. ISSN 2469-7311

<https://doi.org/10.1109/TRPMS.2018.2797484>

(c) 2018 IEEE. Personal use of this material is permitted. Permission from IEEE must be obtained for all other uses, in any current or future media, including reprinting/republishing this material for advertising or promotional purposes, creating new collective works, for resale or redistribution to servers or lists, or reuse of any copyrighted component of this work in other works.

Reuse

Items deposited in White Rose Research Online are protected by copyright, with all rights reserved unless indicated otherwise. They may be downloaded and/or printed for private study, or other acts as permitted by national copyright laws. The publisher or other rights holders may allow further reproduction and re-use of the full text version. This is indicated by the licence information on the White Rose Research Online record for the item.

Takedown

If you consider content in White Rose Research Online to be in breach of UK law, please notify us by emailing eprints@whiterose.ac.uk including the URL of the record and the reason for the withdrawal request.



eprints@whiterose.ac.uk
<https://eprints.whiterose.ac.uk/>

Performance Measurements of the SAFIR Prototype Detector with the STiC ASIC Readout

Max Ahnen, Robert Becker, Alfred Buck, Chiara Casella, Volker Commichau, Diogo di Calafiori, Günther Dissertori, Afroditi Eleftheriou, Jannis Fischer, Member, IEEE, Alexander S. Howard, *Mikiko Ito, Parisa Khateri, Member, IEEE, Jisoo Kim, Werner Lustermaun, Member, IEEE, Christian Ritzer, Ulf Röser, Markus Rudin, Paola Solevi, Charalampos Tsoumpas, Senior member, IEEE, Geoffrey Warnock, Bruno Weber, Matthias Wyss, and Agnieszka Zagodzinska-Bochenek

Abstract—The SAFIR (Small Animal Fast Insert for MRI) PET insert was proposed for quantitative dynamic acquisition inside a preclinical 7T MRI scanner to study kinetics of short-lived tracers. For this purpose, the SAFIR readout should be capable of handling high count rates and achieving excellent timing performance. We evaluated one of the available ASICs for SiPM readout, namely STiC (SiPM Timing Chip) ver. 3.1. In this study, we show the performances of the SAFIR PET detector with the STiC ASIC readout. The SAFIR PET detector consists of an 8×8 array of LYSO $2.1 \text{ mm} \times 2.1 \text{ mm} \times 12 \text{ mm}$ crystals coupled, with optical grease, to an 8×8 array of SiPMs with a $2.0 \text{ mm} \times 2.0 \text{ mm}$ photo-sensitive area. Signals from the individual SiPM channels were digitized by the STiC ASIC. Hit's arrival time and Time-Over-Threshold (TOT) were recorded into time stamps with 50.2 ps LSB. We obtained an average energy resolution of 18.5% FWHM at 511 keV photopeak after TOT non-linearity correction and an average coincidence resolving time (CRT) resolution of 244 ps FWHM with time walk correction that satisfy our requirements specification on the detector performance.

Index Terms—Performance; Photodetector technology; SAFIR; STiC ASIC; SiPM;

Manuscript received September 21, 2017; revised November 19, 2017; accepted December 20, 2017. Date of current version January 20, 2018. This work was supported in part by the ETH Zurich Foundation through ETH Research Grant ETH-30 14-2.

*This manuscript was written by Mikiko Ito (e-mail: mikiko.ito@cern.ch). The authors in this paper were listed in alphabetical order. (Corresponding author: Mikiko Ito)

M. Ahnen, R. Becker, C. Casella, V. Commichau, D. D. Calafiori, G. Dissertori, J. Fischer, A. S. Howard, M. Ito, P. Khateri, W. Lustermaun, C. Ritzer, U. Röser, A. Zagodzinska-Bochenek are with the Institute for Particle Physics and Astrophysics, ETH Zürich, Switzerland.

A. Buck is with the Clinic of Nuclear Medicine, University of Zürich, Switzerland.

A. Eleftheriou, G. Warnock, B. Weber, M. Wyss are with the Institute for Pharmacology and Toxicology, University of Zürich, Switzerland.

M. Rudin is with the Institute for Biomedical Engineering, ETH Zürich, Switzerland.

P. Solevi is with the Institute of Medical Technology, Otto-von-Guericke University Magdeburg, Germany.

C. Tsoumpas is with the Leeds Institute of Cardiovascular and Metabolic Medicine, University of Leeds, United Kingdom.

J. Kim is with the Department of Nuclear and Quantum Engineering, KAIST, South Korea.

I. INTRODUCTION

COMBINED PET/MRI is considered to be more powerful than combined PET/CT for pre-clinical studies because MRI is able to provide functional information (functional MRI, MR spectroscopy, and perfusion measurements) as well as anatomical information with high spatial resolution and the best soft tissue contrast [1]. In addition to the multi-parametric imaging, PET/MR allows simultaneous data acquisition. For those reasons, pre-clinical PET/MR scanners has been actively developed by several research groups [2-12].

One of the benefits of simultaneous PET/MR acquisition is that temporally varying multi-functional information from PET and MRI can be cross-validated or monitored simultaneously, for example, blood flow by PET and blood oxygenation by fMRI or blood oxygenation by fMRI and tracer metabolism in the brain by PET [1].

PET imaging of O-15 water is the gold standard for measuring blood flow in vivo. However, because of its short half-life (122 sec), dynamic PET imaging of O-15 water suffers from the trade-off between temporal resolution and counting statistics; short scan durations are used to achieve high temporal resolution, but it often results in low counting statistics and low signal-to-noise ratio [13, 14].

The SAFIR PET scanner is being designed for use in a pre-clinical 7T MRI scanner (Bruker BioSpec 70/30 USR) for the simultaneous PET/MR acquisitions. This system was proposed for kinetic modeling studies of radiation tracers with short half-life such as O-15 water in order to achieve both high temporal resolution and high counting statistics. For the purpose, the time frame of dynamic image acquisition will be ~2-5 sec to capture fast dynamics. Very high activity of up to 500 MBq will be injected into a small animal to achieve high counting statistics in the short time frame. Data acquisition at such high count rates is very challenging because of dead time and pile-up effects and high random contributions [15]. None of the existing pre-clinical PET scanners can handle such high-rate data.

Figure 1 shows the SAFIR PET insert which has an inner diameter of 130 mm, an outer diameter of 200 mm, and an axial Field-Of-View (FOV) of 180 mm. The PET detector heads (scintillator crystals coupled to SiPMs) and the readout-

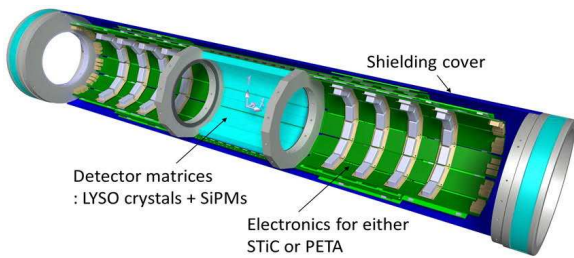


Fig. 1. The SAFIR PET scanner composed of detector heads, ASICs, FPGAs, and power converters.

chips are located at the middle of the MR bore, while FPGAs and power converters are located outside the imaging FOV. A liquid-based cooling system is incorporated to maintain a stable temperature. The inner and outer cylinder are made out of carbon fiber composite materials for shielding.

The SAFIR PET detector employs a one-to-one coupling design of scintillation crystals and photo-sensors in order to avoid dead time and pile-up effects at high count rates. Five surfaces of individual crystals are glued to Enhanced Specular Reflectors (ESR from 3M Optical Systems), and the uncovered crystal surface is coupled to a SiPM. Signals of the individual SiPMs are read out and digitized by application specific integrated circuit (ASIC) chips. This detector design results in the reduction of counts per channel compared to conventional PET block-detectors which utilize light sharing schemes. Conventional block detector designs offer advantage of significant reduction of the readout channels, but on the other hand the counts per channel significantly increases. Based on a Monte Carlo simulation study [16], the average count per channel for the SAFIR PET geometry was estimated to be ~ 40 kHz at 500 MBq activity.

In addition, coincidence events will be acquired using a narrow coincidence time window of ~ 500 ps in order to reduce the random contributions. It requires the SAFIR PET detectors to have excellent timing resolution (< 300 ps FWHM). In a previous simulation study to evaluate the SAFIR PET performances according to National Electrical Manufacturers Association (NEMA) NU-4 2008 standards, we calculated Noise Equivalent Count Rates (NECR) as a function of total activity with various coincidence time windows [16]. The results demonstrated that the NECR values dramatically increased when using narrower coincidence windows (≤ 500 ps). The NECR versus total activity curves continue increasing up to 500 MBq without dead time effect. Using a coincidence time window of 500 ps, the signal-to-noise ratio can be improved by reducing random contributions. In order to fulfill such requirements, a fast electronics with high count rate capability is required [17].

We consider several ASICs for the SAFIR readout. One of the candidates is STiC ASIC ver. 3.1 developed by KIP Heidelberg [18]. Recently, we have assessed the high-rate capability of the STiC ASICs using ^{18}F -FDG with the high activity equivalent to 500 MBq at the SAFIR geometry in the previous high-rate study [19]. Although a different crystal size was used in the high-rate study, counting performance of the

STiC ASICs was extrapolated with correction of the crystal size and geometric factor of the test setup. STiC showed a linear counting response up to a single channel rate of 100 kHz obtained at 500 MBq activity in the SAFIR PET geometry.

In this study, we evaluated the detector performance of the SAFIR PET prototype; output non-linearity due to the SiPM device saturation, light diffusion within a block, and energy- and timing-performances of the SAFIR PET prototype with the STiC readout. Our detector requirements specification is an energy resolution of less than 20% and the CRT resolution of less than 300 ps FWHM with the small pixel size of the detector (~ 2 mm \times ~ 2 mm).

II. MATERIALS AND METHODS

A. The SAFIR Prototype Detector

The SAFIR PET detector is composed of an 8×8 array of Lutetium Yttrium OxyorthoSilicate (LYSO) 2.1 mm \times 2.1 mm \times 12 mm crystals (Agile Technologies) and an 8×8 array of SiPMs with an effective photo-sensitive area per channel of 2.0 mm \times 2.0 mm (Hamamatsu S13361-2050AE-08), as shown in Fig. 2(a). The SiPMs have 1584 micro-cells with a micro-cell size of 50 μm . All surfaces of the LYSO crystals are mechanically polished and the surfaces of the crystals are glued on ESR reflectors except one surface facing the SiPM surface. In a crystal array, both sides of the ESR reflectors are glued to the crystals. All crystals are one-to-one coupled to the SiPMs using optical grease. The crystal pitch is 2.2 mm which matches with the SiPM-channel pitch of 2.2 mm.

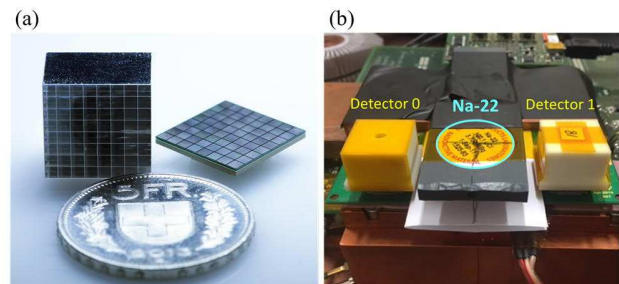


Fig. 2. (a) An 8×8 array of LYSO scintillation crystals and an 8×8 array of SiPMs and (b) the test setup using two SAFIR PET detectors each connected to one STiC ASIC chip and a Na-22 point source placed between two detectors.

B. VME Setup to Measure SiPM Device Saturation and Light Diffusion in a Block

Since the SAFIR detector head utilizes the “one-to-one” coupling design, a large amount of scintillation light is focused on one SiPM channel which has the limited number of micro-cells. It causes SiPM output saturation due to high photon flux rate. On the other hand, even with the “one-to-one” coupling, scintillation light can spread within a detector block because of two main causes: (i) light diffusion through glue- and epoxy-layers on a SiPM array and (ii) light transmission through ESR reflectors optically bonded to crystals due to the quenched reflectivity [20]. Thus, we

investigated the non-linear signal output due to the SiPM device saturation and light diffusion within a block for the SAFIR detector, using a 16 channel Charge-to-Digital Converter (QDC VME module, CAEN v792). Because of the available channel number of the QDC module, a 4×4 detector head composed of a 4×4 crystal array and a 4×4 SiPM array was built and used for the QDC measurements. Except of the number of elements ($64 \rightarrow 16$ channels), all materials and dimensions are same as the prototype detector head described in the section II-A.

We performed three measurements, Lu-176 intrinsic radiation, Na-22 radiation, and single photon measurements. The output non-linearity of the SAFIR detector head was evaluated by comparing the measured signal charges to the corresponding gamma energies for four photo-peaks, 202 keV and 307 keV for Lu-176 intrinsic, and 511 keV and 1275 keV for Na-22 radiation. Light diffusion within a block was calculated from the Na-22 measurements when 511 keV gamma rays interacted with one of crystals in a block. Single photon spectrum was used for calculating the SiPM gain. The SiPM gain is needed for calculating the number of observed photoelectrons corresponding to the measured charge values.

The analog signals from the SiPMs were connected to a 16 channel pre-amplifier with two outputs per channel (for the QDC and a trigger board). The pre-amplifier offers two different gains which can be selected for interesting signal levels: low gain for radiation measurements (> 1000 photons), and high gain for the single photon measurements. The amplified signal charges from 16 channels were integrated and recorded in the QDC module while the QDC were receiving “GATE” input. In the three measurements, different trigger signals were used for the “GATE” input.

For the Lu-176 intrinsic measurement, a trigger signal for the detector head (from a trigger board) was connected to the “GATE” input. In the trigger board, the amplified signals from 16 channels were connected to a leading-edge-discriminator and “OR” circuit to generate the trigger signal for the detector head.

Na-22 radiation was measured by coincidence detection with a one-channel reference detector composed of a $2 \text{ mm} \times 2 \text{ mm} \times 10 \text{ mm}$ LYSO crystal and a one-channel SiPM. Na-22 point source was placed between the detector head and the reference detector. Trigger signals for the two detectors were generated in the above-mentioned process, and combined via “AND” circuit to generate a coincidence trigger in the trigger board. The coincidence trigger was connected to the “GATE” input for the Na-22 radiation measurement.

For the single photon measurement, without scintillation crystals, SiPM devices were illuminated by a blue light emitting diode (blue LED) which was operated, with 5 ns rise/fall time and 20 ns pulse width, by a pulse generator (Agilent 22350A). A sync pulse of the pulse generator was used as a trigger signal for measuring single photons, and connected to the “GATE” input. For all measurements mentioned in this section, a pulse width of “GATE” input was 300 ns and SiPMs were operated at the recommended

operation voltage by Hamamatsu (over-voltage of 3V).

C. STiC ver.3.1

STiC is a 64-channel readout ASIC specifically developed by the EndoTOFPET-US project to achieve excellent timing performance with SiPM devices [18]. Each channel has two discriminators; i) a low-threshold (T-threshold) discriminator that generates a trigger of hit’s arrival by the leading edge of the signal pulse crossing the low-threshold; and ii) a high-threshold (E-threshold) discriminator that generates a trigger of valid hits. The time difference between the leading edge with T-threshold and the falling edge of the pulse crossing E-threshold is used for Time-Over-Threshold (TOT) measurements as signal charge information. STiC provides a so-called “linearized TOT” method which provides a better linearity than conventional TOT methods. The “linearized TOT” was implemented by charge collection and linear discharge ramp [21]. In other words, the signal charge is stored on the SiPM and is discharged with constant current. As a consequence the total discharge time is proportional to the total detected charge. The TOT response therefore becomes linearized to the total signal charge providing better energy performance. The amount of the discharge current can be adjusted by a STiC configuration parameter, namely “inputBias”. The TOT value and the hit arrival time are recorded into time stamps with 50.2 ps LSB width. The STiC chip has two TDC modules in which Phase Lock Loop (PLL) is used to lock a 16-stage voltage controlled ring oscillator (VCO) to a reference clock with 625 MHz and the VCO output feeds up a 15-bit coarse counter [22]. The state of the VCO (as fine counter) and the coarse counter value are stored for the arrival time and the TOT of each hit.

D. STiC Readout Setup to Measure Detector Performance

Figure 2(b) shows the test setup to measure detector performances with STiC readout. Each detector head (8×8 array) was connected to a 64-channel STiC readout ASIC for an individual readout of each SiPM channel. Two ASIC chips were mounted on a thermal pad coupled to a water-cooled copper plate to maintain a stable temperature, and connected to the mother board. The two ASICs were synchronized through the mother board and their digital signals were read out by an FPGA on the mother board; the mother board and the FPGA readout were provided by KIP Heidelberg. More details of the mother board and DAQ hardware can be found in [23, 24].

When the detectors and ASIC chips were powered, the temperatures on the thermal pad and on the PCB board near the ASIC chip were $18.5 \text{ }^\circ\text{C}$ and $25 \text{ }^\circ\text{C}$, respectively. SiPMs were operated at 55.6V (V_{op}) corresponding to an over-voltage ($\Delta V = V_{op} - V_{br}$) of $\sim 3.0 \text{ V}$. A Na-22 radiation point source was placed in the middle of the two detectors, and irradiated at the side of the detectors.

TDCs on the STiC ASICs were calibrated while injecting test pulses with a pre-fixed period and calculating the period

of the test pulses. The TDC configurations were determined to find the known period and to ensure the PLL to be locked. The differential-non-linearity (DNL) of the individual TDC stages was measured, and the integral-non-linearity (INL) was calculated. The TDC non-linearity (DNL/INL) was corrected in an off-line process using the calculated compensation look-up table.

For optimizing detector performance, we adjusted three STiC configuration parameters for individual channels; T-thresholds, E-thresholds, and the parameter “inputBias”. TOT spectra of Lu-176 intrinsic and Na-22 radiations were obtained to measure the TOT non-linearity to the gamma ray energies. This non-linearity includes two effects: non-linear response of TOT method and SiPM device saturation due to the small total number of micro-cells. The measured TOT non-linearity was used to calculate a linearized energy spectrum. Energy resolutions were calculated after the non-linearity correction.

Timing performance was evaluated with coincidence detections as shown in Fig. 2(b). Singles data were acquired in list mode, and the coincidence events were generated in the off-line process applying various energy windows, $\pm 1.5\sigma$ around 511 keV photo-peaks, 350-650 keV, and 250-750 keV, and a coincidence time window of 10 ns. Time walk effects were measured and corrected for calculating coincidence resolving time (CRT).

III. RESULTS AND DISCUSSIONS

In the following sections A and B, we report the SiPM device saturation and light diffusion within a block measured on the QDC VME setup. In the following sections C, D, and E, we show the energy and timing performances measured by STiC readout with the same configuration (sections III-C and III-D) and with various configurations (section III-E).

A. SiPM device saturation

Figures 3(a) and 3(b) show QDC spectra of Lu-176 intrinsic and Na-22 radiations measured from the same channel of the SAFIR detector. For four photo-peaks in the two spectra, 202 keV and 307 keV in the Lu-176 spectrum and 511 keV and 1275 keV in the Na-22 spectrum, the measured charge outputs (QDC values) were compared to the corresponding gamma-ray energies for the evaluation of the SiPM device saturation.

Figure 4 shows the non-linear response of observed photoelectrons versus gamma-ray energy. The number of observed photoelectrons was calculated from the measured charge value divided by the SiPM gain, pre-amplifier gain, and electron charge. Four data points were fitted by a negative exponential function in equation (1) which describes the SiPM saturation behavior in terms of a relationship among the number of photons that arrived at the sensor, the number of fired micro-cells, and the total number of micro-cells per a channel [25].

$$N_{pe} = a(1 - \exp(-bE)) \quad (1)$$

$$N'_{pe} = a \cdot b \cdot E \quad (2)$$

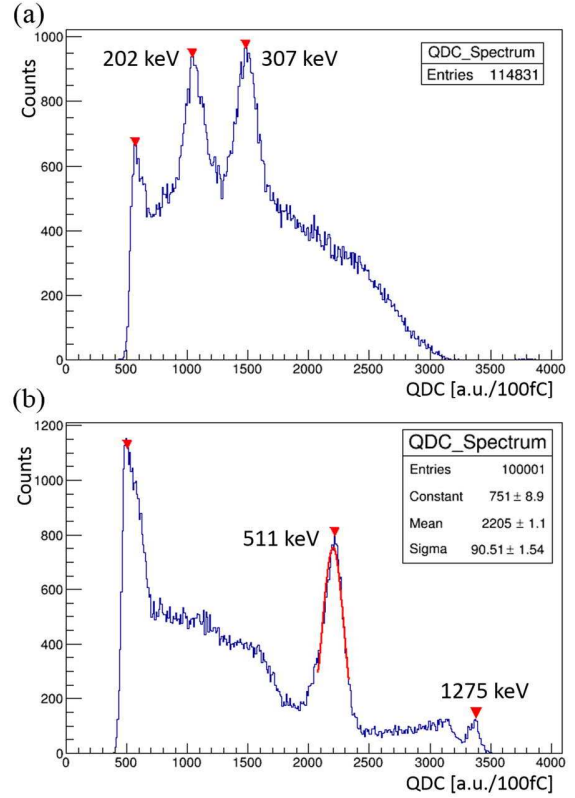


Fig. 3. QDC spectra of (a) intrinsic Lu-176 radiations included in the LYSO scintillation crystals and (b) a Na-22 radiation source.

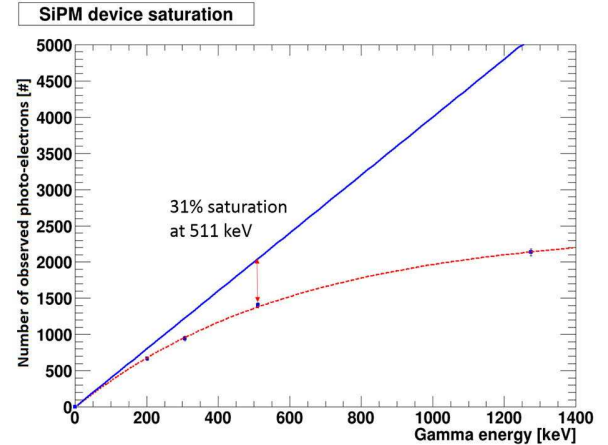


Fig. 4. The non-linearity of the number of observed photo-electrons versus gamma-ray energy in keV. The fitted equation (1) was shown in the dashed red line and the calculated equation (2) in the solid blue line.

where N_{pe} is the number of observed photon-electrons, E is the corresponding gamma energy, and N'_{pe} is the ideal number of observed photo-electrons calculated by assuming if there were no saturations in SiPMs.

In the Fig. 4, the fitted equation (1) was shown in the dashed red line and the calculated equation (2) in the solid blue line. The SiPM device saturation was estimated to be ~31% at 511 keV gamma ray energy.

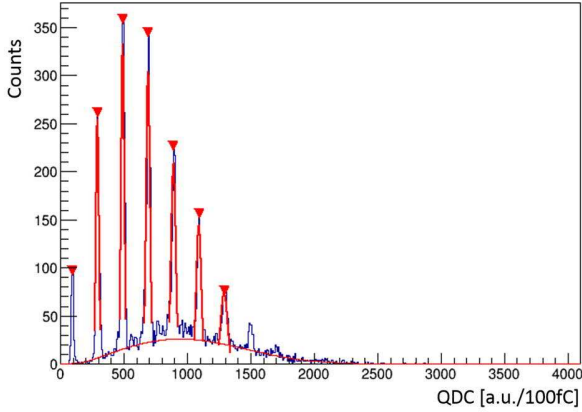


Fig. 5. Single photon spectrum of a 2 mm x 2 mm SiPM measured with blue LED light emission.

For the 1275 keV photo-peak events, we observed a larger number of photo-electrons than the total number of micro-cells per channel. Because the SiPM produced by Hamamatsu has faster recovery time (50 ns) than the duration of one event (~200 ns), recovering or recovered cells can contribute to increasing signal [26]. The SiPM gain used for calculating the number of observed photoelectrons was experimentally measured from a single photon spectrum in Fig. 5. The single photon QDC spectrum was measured from the same SiPM channel without crystals while illuminated by blue LED. SiPM gain was calculated to be 1.95×10^6 at 22°C from the charge difference between two peaks divided by electron charge and pre-amplifier gain. The SiPM gain was expected to be 1.7×10^6 at 25 °C at the recommended operation voltage provided in a data sheet. The difference between the measured gain and the expected gain was caused by the temperature difference ($\Delta T = 3$ °C).

B. Light diffusion within a block

In this section, we show light diffusion within a block measured by the QDC VME module. 2-D signal distribution on the 4 x 4 array was shown in Fig. 6. The signal distribution was obtained when 511 keV photo-peak events were observed at channel C-2. Text shows a percentage ratio (%) of the given signal to the total sum of 16 channel signals. About 64% of the total signal, which is corresponding to ~1400 photoelectrons with ~31% saturation (Fig. 4), was observed at the interacted channel C-2. The rest of 36% of the total signal, which is corresponding to ~787 photo-electrons, were observed on the neighbor channels. It indicated that our SAFIR detector has light diffusion within a block probably due to the glue- and epoxy-layers between crystals and SiPMs and the quenched reflectivity of ESR reflectors glued on the both sides. It requires E-thresholds to be set high enough to reject the neighbor signals caused by light diffusion.

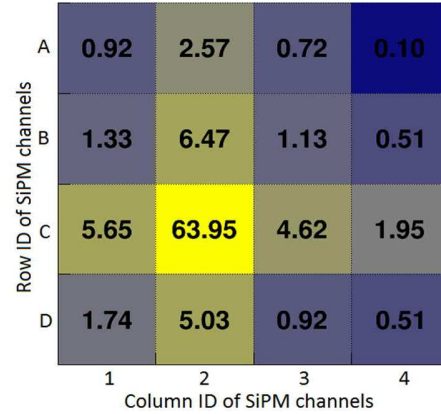


Fig. 6. 2-D signal distribution on a 4 x 4 channel array when 511 keV photo-peak events were detected at channel C-2. Text shows a percentage ratio of the given signal to the total sum of 16 channel signals.

C. TOT Spectra and Energy Performance

This section describes TOT and energy performance obtained with the same STiC configurations, specifically the DAC value of 10 for T-thresholds and 11 for “inputBias” over all channels and E-thresholds around 50 keV to 100 keV adjusted for the individual channels. An event is valid if its signal level is above the E-threshold, and its arrival time is determined with the T-threshold. The bandwidth of the input stage and the TOT response depend on the “inputBias” parameter.

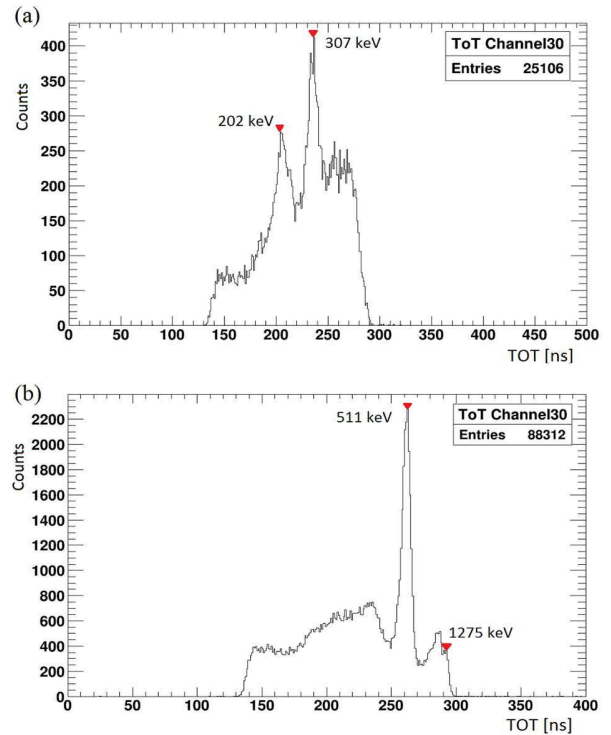


Fig. 7. TOT spectra of (a) intrinsic Lu-176 radiations included in the LYSO scintillation crystals and (b) a Na-22 radiation source measured from the same channel (Ch. 30) with the same STiC configuration.

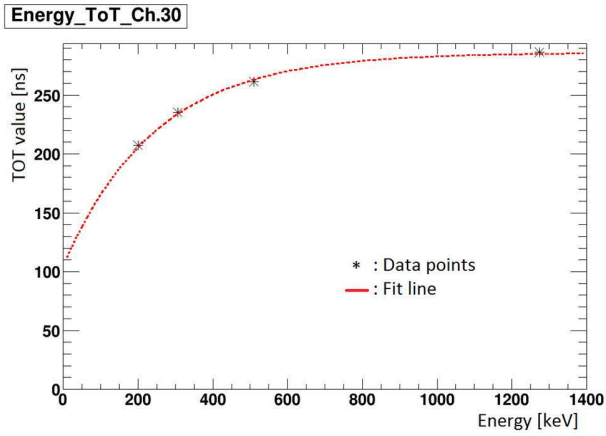


Fig. 8. The non-linearity of the TOT value in ns versus gamma-ray energy in keV for channel 30. Four data points were fitted by equation (3), as shown in the dashed red line.

Figures 7(a) and 7(b) show TOT spectra of the Lu-176 intrinsic and the Na-22 radiations obtained from the same channel (ch.30), respectively. The central values of the four photo-peaks corresponding to 202 keV, 307 keV in the Lu-176 intrinsic spectrum, 511 keV, and 1275 keV in Na-22 spectrum were used for estimating the TOT non-linearity, as shown in Fig. 8. These four data points were fitted with a negative exponential function in equation (3) described by the dashed red line.

$$\text{TOT}(E) = c + a(1 - \exp(-bE)) \quad (3)$$

The equation (3) was defined by the SiPM non-linear response like the equation (1). The inverse of the equation was applied to the TOT values in order to obtain the linearized energy spectrum in Fig. 9. The energy resolution for the channel 30 was calculated to be 17.9% at FWHM for 511 keV photo-peak after non-linearity correction. The TOT non-linearity response was measured and corrected on a crystal-by-crystal basis. Figures 10 and 11 show the TOT non-linearity curves and the linearized energy histograms, respectively, for one-quarter of total number of crystals (from ch. 48 to ch. 63).

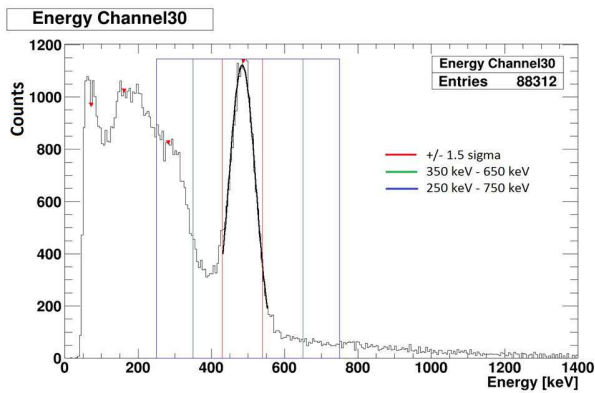


Fig. 9. The linearized energy spectrum in keV for channel 30. Three energy windows were described, $\pm 1.5\sigma$ around 511 keV photo-peak in the red line, 350 keV – 650 keV in the green line, and 250 keV – 750 keV in the blue line.

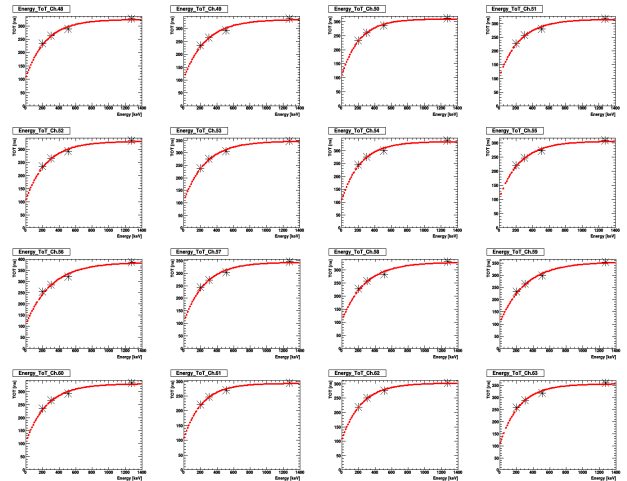


Fig. 10. TOT non-linearity curves for 16 channels (channel 48 - 63).

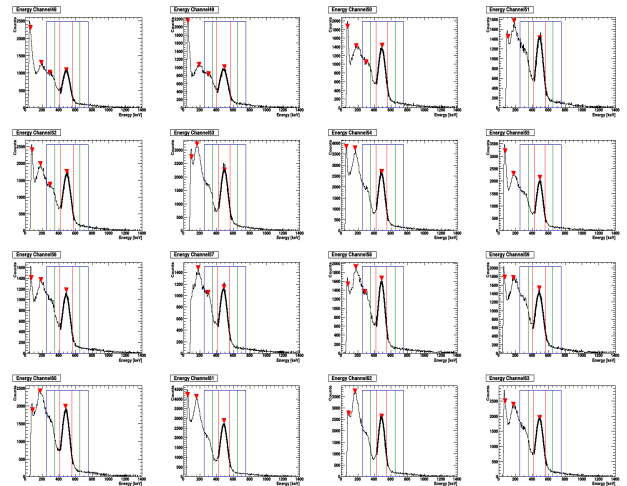


Fig. 11. The linearized energy histograms in keV for 16 channels (ch. 48 - 63) with various energy windows; $\pm 1.5\sigma$ around 511 keV photo-peak in red line, 350 keV – 650 keV in green line, and 250 keV – 750 keV in blue line.

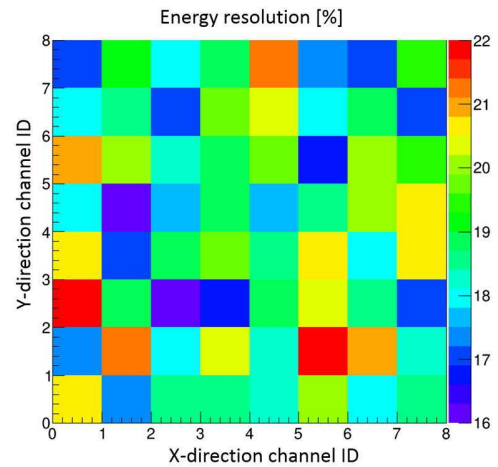


Fig. 12. Energy resolutions after non-linearity correction for 64 channels in a detector were shown in the 2D color histogram.

In Fig. 11, three kinds of energy windows were described in the energy histograms; $\pm 1.5\sigma$ around 511 keV photo-peak in the red line, 350 keV – 650 keV in the green line, and 250 keV – 750 keV in the blue line. Figure 12 shows the energy resolutions for all 64 channels. The range of the energy resolutions were from 16% to 21%. An average energy resolution of 18.9% was calculated over all channels in the two detectors.

D. CRT Measurements with time walk correction

CRT performance shown in this section was obtained with the same STiC configurations as the section III-C.

Since a time-trigger pulse was generated by a leading-edge-discriminator in STiC, the triggered time was shifted by signal amplitude. This effect is called “time walk”. We observed time walk effect in STiC using a wide-open energy window (100 keV – 800 keV) for one detector and a narrow energy window ($\pm 1.5\sigma$ around 511 keV) for the other detector. Time walk curves for 16 crystals (one-quarter of the total number) were shown in Fig. 13. Coincidence-event counts varies depending the crystal location because of the test setup in which two detectors were irradiated at the side, as shown in Figure 2(b). Coincidence time differences (delta T calculated by $t_0 - t_1$, where t_0 is time stamp for detector #0 and t_1 for detector #1) were shifted as a function of gamma-ray energy. These time walk curves were obtained by a crystal by crystal basis, and were fitted by a third degree polynomial function. Time walk between the given energy and 511 keV photo-peak was calculated by the fitted function and corrected on an event-by-event basis.

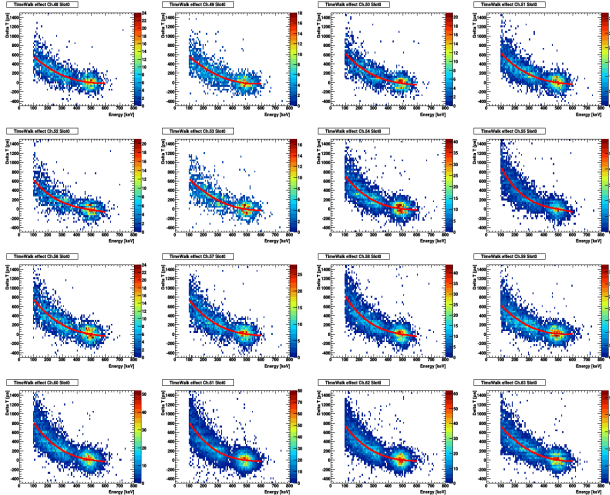


Fig. 13. Time walk effect for 16 crystals (channel 48 – 63). Coincidence time difference (Delta T) was shifted as a function of energy.

CRT distributions were generated for individual crystal-to-crystal pairs between two detectors by using a coincidence time window of 10 ns and three kinds of energy windows, $\pm 1.5\sigma$ around the 511 keV photo-peak, 350 keV – 650 keV, and 250 – 750 keV. Figure 14 shows the CRT distribution of one coincidence pair between channel 2 in detector #0 and channel 30 in detector #1. This was calculated by energy

window of $\pm 1.5\sigma$ around 511 keV with time walk correction. CRT sigma of 97.1 ps (229.2 ps FWHM) was obtained by fitting the CRT histogram with a Gaussian function. Figure 15 shows the CRT sigma versus the entries of the corresponding CRT histograms for all coincidence pairs that have more than 100 entries. The average CRT resolution with time walk correction was estimated to be ~ 103 ps sigma (~ 244 ps FWHM) over 381 crystal pairs, shown by the fitted red line in Fig. 15. Because of the geometric effect of the coincidence measurements using a Na-22 point source between two detectors (Fig. 2(b)), limited number of crystal pairs can get coincidence events.

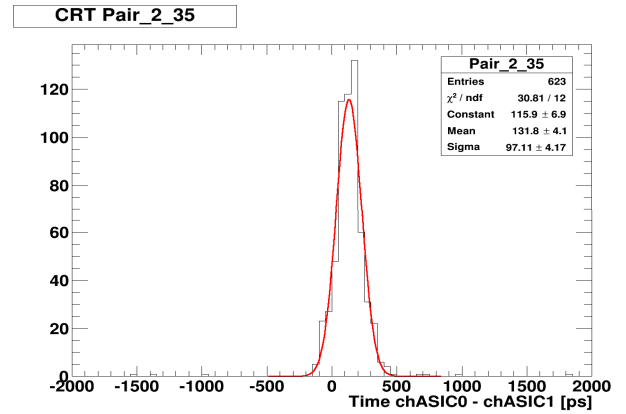


Fig. 14. CRT histogram of one crystal pair between channel 2 in the detector #0 and channel 35 in the detector #1.

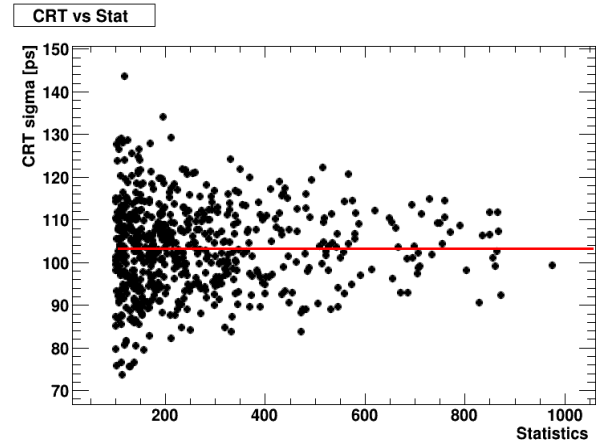


Fig. 15. CRT sigma vs. entries in the CRT distribution for individual crystal pairs

In the table I, average CRT resolutions with/without time walk correction for different energy windows were summarized. Time walk effect increases as using wider energy windows, time walk correction is important for the wide energy window such as 250 keV – 750 keV. Average CRT resolutions with time walk correction were calculated to be 244 ps FWHM with energy window of $\pm 1.5\sigma$ around 511 keV photo-peak, 254 ps FWHM with energy window of 350 keV – 650 keV, and 288 ps FWHM with energy window of 250 keV – 750 keV.

TABLE I
AVERAGE CRT RESOLUTIONS WITH VARIOUS ENERGY WINDOWS
WITH/WITHOUT TIME WALK CORRECTION

Energy window	Average CRT resolution at FWHM without time walk correction	Average CRT resolution at FWHM with time walk correction
$\pm 1.5 \sigma$	246 ps	244 ps
350 keV – 650 keV	267 ps	254 ps
250 keV – 750 keV	365 ps	288 ps

E. Detector performance with various STiC configurations

In this section, we show energy and CRT performances obtained with various STiC configurations. TOT spectra in Figures from 16(a) to 16(e) were measured with “inputBias” parameter of 3, 7, 11, 15, and 19, respectively, while T- and E-thresholds were fixed.

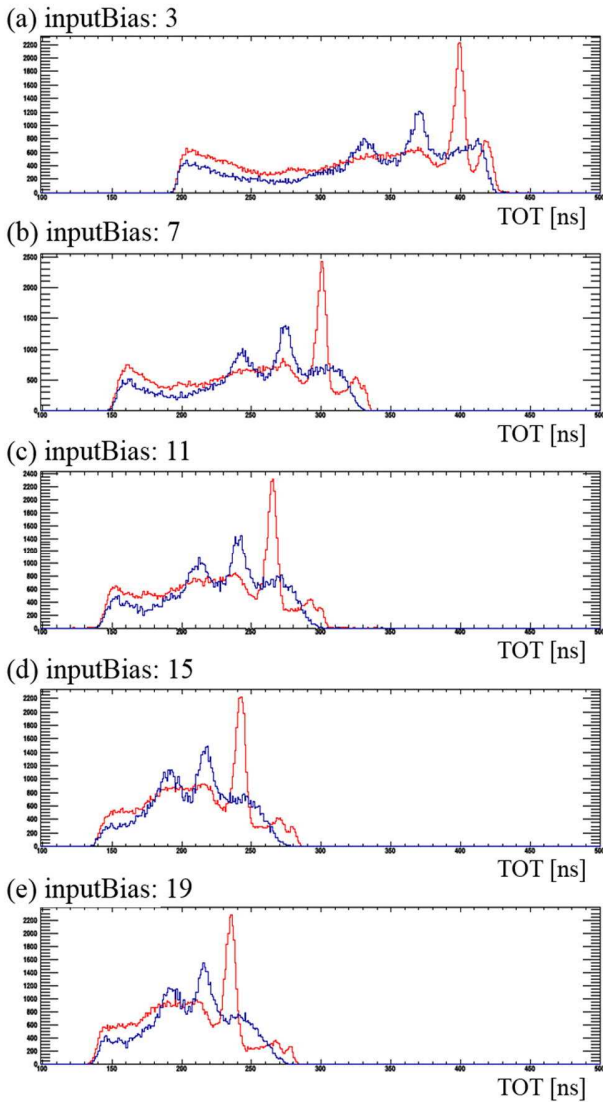


Fig. 16. TOT spectra of Lu-176 intrinsic in blue and Na-22 in red with the “inputBias” parameters of (a) 3, (b) 7, (c) 11, (d) 15, and (e) 19.

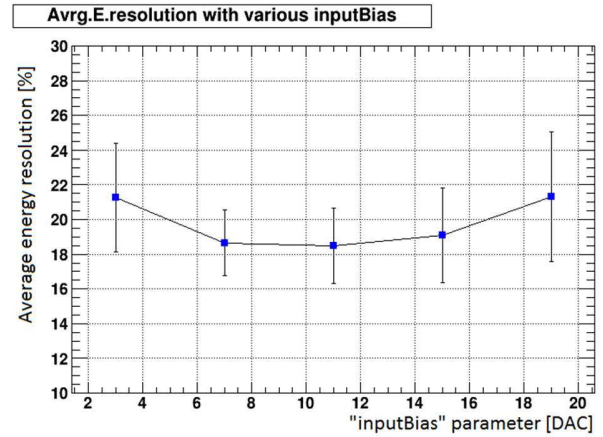


Fig. 17. Average energy resolution over 64 channels versus STiC configuration setting of “inputBias” parameter. Error bars show the standard deviation of the populations of energy resolutions over 64 channels.

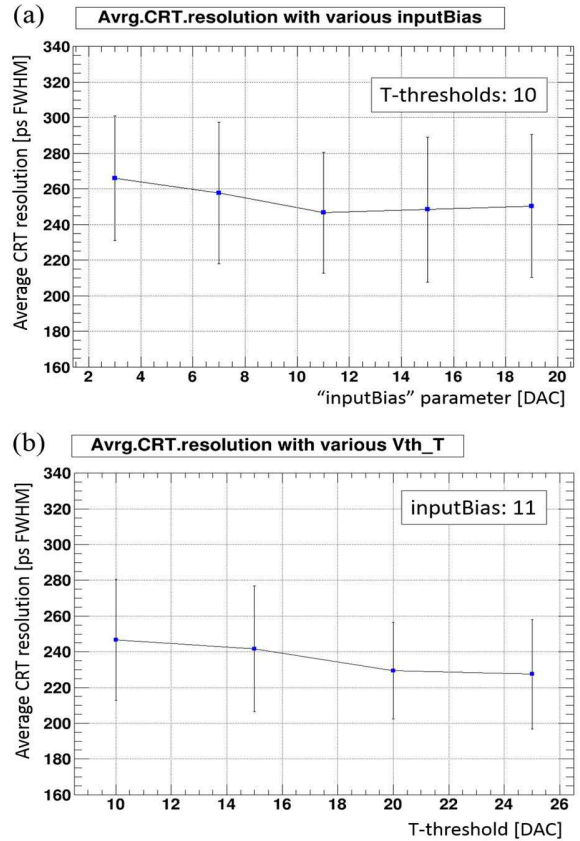


Fig. 18. Average CRT FWHM resolution with (a) various “inputBias” while fixing T-thresholds to be 10 and with (b) various T-thresholds settings while fixing “inputBias” to be 11.

Fig. 16 indicated that a linearity of TOT response can be improved by adjusting “inputBias” parameter for an interesting signal level. When the “inputBias” was set to the small value, TOT response shows a good linearity for small signals, but saturation for large signals. When the “inputBias” was set to large value, TOT has better linearity for large signals.

Average energy resolution as a function of “inputBias” setting was shown in Figure 17. The energy resolutions were calculated after the TOT non-linearity correction described in section III-C. Good energy resolutions less than 20% were obtained in a wide range of “inputBias” setting from 7 to 15.

Average CRT FWHM resolutions as functions of “inputBias” and T-threshold were shown in Figures 18(a) and 18(b), respectively. The Larger DAC value of T-thresholds corresponds to lower threshold. The average CRT resolutions were calculated with energy window of $\pm 1.5 \sigma$ around 511 keV and without time walk correction.

Based on the results in Figures 17 and 18(a), DAC setting of 11 for “inputBias” parameter looks suitable for signal level of the SAFIR detector in terms of energy and timing performances. We obtained an average energy resolution of 18.5% and average CRT resolution of 246 ps FWHM with the “inputBias” of 11 and T-thresholds of 10 without time walk correction. In Figure 18(b), low timing threshold just above the noise level (DAC value of 25) leads to about 20 ps improvement of CRT resolution. When using a larger DAC value than 25 for T-thresholds, several channels started detecting noise which causes degradation in TOT response as well as in CRT performance. We concluded that STiC chip is starting to trigger noise with DAC values greater than 25 for T-thresholds.

IV. SUMMARY AND OUTLOOK

In this study, we investigated the performance of the STiC v3.1 ASIC with the foreseen SAFIR detectors; output non-linearity due to the SiPM device saturation, light diffusion within a block, and energy- and timing-performances of the SAFIR prototype detector with the STiC readout. A SiPM device saturation of ~31% at 511 keV gamma energy was observed due to high photon flux focused on one SiPM channel which has the limited number of micro-cells. On the other hand, even with the one-to-one coupling, we observed that scintillation light was spread over neighbor channels probably through glue- and epoxy-layers on a SiPM array and ESR reflector with quenched reflectivity. In order to avoid detecting those light diffusion hits, E-threshold of individual channels need to be adjusted high enough to avoid detecting hits originating from light spread to neighbors. Energy and CRT performances were measured by the STiC readout with different configurations. This measurement demonstrates that STiC provides good energy (TOT) and excellent timing performance for a wide range of configuration setting. We obtained the average energy resolution of 18.5% after TOT non-linearity correction and the average CRT resolution of 244 ps FWHM with time walk correction, which satisfy our requirements on the detector performances. Next, the detector performance will be evaluated inside the MR scanner in order to check the MR-compatibility of the STiC chip.

V. ACKNOWLEDGMENT

We thank Hans-Christian Schulz-Coulon and his group, in particular Tobias Harrion and Wei Shen from the Kirchhoff Institute of Physics of University Heidelberg, for their continues support in using the STiC ASICs, for providing the STiC ASICs and mounting them onto our carrier boards, as well as for providing the mother board readout system.

REFERENCES

- [1] H. F. Wehrli, M. S. Judenhofer, S. Wiehr, and B. J. Pichler, “Pre-clinical PET/MR: technological advances and new perspectives in biomedical research”, *Eur. J. Nucl. Med. Mol. Imaging*, 36, S56-S68, 2009.
- [2] Y. Shao, et al., “Simultaneous PET and MR imaging”, *Phys Med Biol*, 42 (10), pp. 1965-1970, 1997.
- [3] P. K. Marsden, et al., Simultaneous PET and NMR, *Br. J. Radiol*, 75, S53-S59, 2002.
- [4] M. S. Judenhofer, et al., “Simultaneous PET-MRI: a new approach for functional and morphological imaging”, *Nat. Med.* 14 (4), pp. 459-465, 2008.
- [5] C. Catana, D. Procissi, Y. Wu, M. S. Judenhofer, J. Qi, B. J. Pichler, et al., “Simultaneous in vivo positron emission tomography and magnetic resonance imaging.” *Proc. Natl. Acad. Sci. USA*, 105 (10), pp. 3705-3710, 2008.
- [6] R. R. Raylman, S. Majewski, S. K. Lemieux, S. S. Velan, B. Kross, V. Popov, et al., “Simultaneous acquisition of magnetic resonance spectroscopy (MRS) data and positron emission tomography (PET) images with a prototype MR-compatible, small animal PET imager”, *J. Magn Reson.* 186 (2), pp. 305-310, 2007.
- [7] S. Yamamoto, K. Mazumoto, and M. Senda, “Development of a multi-slice dual layer MR-compatible animal PET system using DOI detectors”, *Supplement to the Journal of Nuclear Medicine*, 48, 89P, 2007.
- [8] H. P. Schlemmer, et al., “An integral MR/PET system: prospective applications”, *Abdom Imaging* 2008 doi:10.1007/s00261-008-9450-2.
- [9] A. J. Lucas, R. C. Hawkes, R. E. Ansorge, G. B. Williams, R. E. Nutt, J. C. Clark, T. D. Fryer, and T. A. Carpenter, “Development of a combined microPET-MR system,” *Technol. Cancer Res. Treat.* 5(4), pp. 337-341, 2006.
- [10] J. E. Mackewn, C. W. Lerche, B. Weissler, K. Sunassee, R. T. M. de Rosales, A. Phinikaridou, A. Salomon, R. Ayres, C. Tsoumpas, G. M. Soutanidis, P. Gebhardt, T. Schaeffer, P. K. Marsden, and V. Schulz, “PET performance evaluation of a pre-clinical SiPM-based MR-compatible PET scanner”, *IEEE Trans. Nucl. Sci.* 62 (3), pp. 784-790, 2015.
- [11] S. Yamamoto, H. Watabe, Y. Kanai, M. Aoki, E. Sugiyama, T. Watabe, M. Imaizumi, E. Shimosegawa, J. Hatazawa, “Interference between PET and MRI sub-systems in a silicon-photomultiplier-based PET/MR system”, *Phys. Med. Biol.* 56 (13), pp. 4147-4159, 2011.
- [12] G. B. Ko, H. S. Yoon, K. Y. Kim, and J. S. Lee, “Simultaneous multiparametric PET/MRI with silicon photomultiplier PET and ultra-high field MRI for small animal imaging”, *J. Nucl. Med.*, 57 (8), pp. 1309-1315, 2016.
- [13] A. Rahmin, and J. Tang, “Four-dimensional (4D) image reconstruction strategies in dynamic PET: Beyond conventional independent frame reconstruction”, *Med. Phys.* 36, 3654-3670, 2009.
- [14] G. Wang, and J. Qi, “PET image reconstruction using kernel method”, *IEEE Trans. Med. Imaging*, 34 (1), pp. 61-71, 2015.
- [15] D. A. Mankoff, G. Muehllehner, and J. S. Karp, “The high count rate performance of a two-dimensionally position-sensitive detector for positron emission tomography”, *Phys. Med. Biol.*, 34 (4), pp. 437-456, 1989.
- [16] R. Becker, J-P. Cachemiche, C. Casella, G. Dissertori, J. Fischer, A. S. Howard, K. Kramer, W. Lustermann, C. Morel, J. F. Oliver, U. Roser, Q. Wang, and B. Weber, “Monte-Carlo simulation based estimation of NECR, sensitivity and spatial resolution of a novel preclinical PET insert for MR,” *IEEE NSS-MIC Conference Record*, 2015.
- [17] R. Becker, A. Buck, C. Casella, G. Dissertori, J. Fischer, A. Howard, M. Ito, P. Khateri, W. Lustermann, J. F. Oliver, U. Roser, G. Warnock, and B. Weber, “The SAFIR experiment: Concept, status and perspectives,” *Nucl. Instr. Math. Phys. A* 845, pp. 648-651, 2017.

- [18] T. Harion, K. Briggel, H. Chen, P. Fischer, A. Gil, V. Kiworra, M. Ritzert, H.-C. Schultz-Coulon, W. Shen, and V. Stankova, "STiC – a mixed mode silicon photomultiplier readout ASIC for time-of-flight applications," *Journal of Instrumentation*, vol. 9, C02003, Feb. 2014.
- [19] R. Becker, C. Casella, S. Corrodi, G. Dissertori, J. Fischer, A. Howard, M. Ito, and W. Lustermann, "Studies of the High Rate Coincidence Timing Response of the STiC and TOPPET ASICs for the SAFIR PET Scanner *Journal of Instrumentation*, vol. 11, P12001, Dec. 2016.
- [20] F. Loignon-Houle, C. M. Pepin, S. A. Charlebois, and R. Lecomte, "Reflectivity quenching of ESR multilayer polymer film reflector in optically bonded scintillator arrays," *Nucl. Instr. Math. Phys. A* 851, pp. 62-67, 2017.
- [21] V. Stankova, W. Shen, K. Briggel, H. Chen, P. Fischer, A. Gil, T. Harion, V. Kiworra, Y. Munwes, M. Ritzert, and H. Schultz-Coulon, "STiC3-silicon photomultiplier timing chip with picosecond resolution," *Nucl. Instr. Math. Phys. A* 787, pp. 284-287, 2015.
- [22] W. Shen, K. Briggel, H. Chen, P. Fischer, A. Gil, T. Harion, V. Kiworra, M. Ritzert, H. Schultz-Coulon, and V. Stankova, "STiC2-characterization results of a SiPM readout ASIC for time-of-flight applications," *IEEE NSS-MIC Conference Record*, 2013.
- [23] H. Chan, K. Briggel, P. Fischer, A. Gil, T. Harion, Y. Munwes, M. Ritzert, D. Schimansky, H.-C. Schultz-Coulon, W. Shen, and V. Stankova, "A dedicated readout ASIC for time-of-flight positron emission tomography using silicon photomultiplier (SiPM)," *IEEE NSS MIC Conference Record*, 2014.
- [24] T. Harion, "The STiC ASIC: high precision timing with silicon photomultipliers", Ph.D Thesis, Heidelberg University, 2015.
- [25] D. Renker, and E. Lorentz, "Advances in solid state photon detectors," *Journal of Instrumentation*, vol. 4, P04004, Apr. 2009.
- [26] H. Oide, H. Otono, S. Yamashita, T. Yoshioka, H. Hano, T. Suehiro, "Study of afterpulsing of MPPC with waveform analysis", *Proceedings of Science (PD07)*, 008, 2007.